REENTRANT AND FORWARD PHASE DIAGRAMS OF THE ANISOTROPIC $d = 3$ ISING SPIN-GLASS

by

Can Güven

A Thesis Submitted to the
Graduate School of Sciences
in Partial Fulfillment of the Requirements for
the Degree of

Master of Science

in

Physics

Koç University

August, 2008

Koç University

Graduate School of Sciences and Engineering

This is to certify that I have examined this copy of a master's thesis by

Can Güven

and have found that it is complete and satisfactory in all respects,
and that any and all revisions required by the final
examining committee have been made.

Committee Members:

_____

Prof. A. Nihat Berker

_____

Assoc. Prof. F. Gülay Acar

_____

Assist. Prof. Alkan Kabakçıoğlu

Date: _____

To my parents

ABSTRACT

The spatially uniaxially anisotropic $d = 3$ Ising spin glass is solved exactly on a hierarchical lattice. This solution also constitutes a very good approximation to the cubic lattice. Five different ordered phases, namely ferromagnetic, columnar, layered, antiferromagnetic, and spin-glass phases, are found in the global phase diagram. The spin-glass phase is more extensive when randomness is introduced within the planes than when it is introduced in lines along one direction. Phase diagram cross-sections, with no Nishimori symmetry, with Nishimori symmetry lines, or entirely imbedded into Nishimori symmetry, are studied. The boundary between the ferromagnetic and spin-glass phases can be either reentrant or forward, that is either receding from or penetrating into the spin-glass phase, as temperature is lowered. However, this boundary is always reentrant when the multicritical point terminating it is on the Nishimori symmetry line.

ÖZETÇE

Tek eksenli anizotropik üç boyutlu Ising spin camının hiyerarşik örgüde kesin çözümü yapılmıştır. Bu çözüm aynı zamanda kübik örgü için de çok yakın çözümler vermektedir. Global faz diyagramında; ferromanyetik, düzlem modüle, eksen modüle, antiferromanyetik ve spin camı olmak üzere beş farklı düzenli faz bulunmuştur. Düzleme eklenen rasgelelik, tek eksene eklenen rasgelelikle karşılaştırıldığında spin camı fazının daha yoğun olduğu gözlenmiştir. Nishimori simetrisiz, Nishimori simetri çizgileri içeren ve bütünüyle Nishimori simetrisine sahip faz diyagramı kesitleri incelenmiştir. Ferromanyetik ve spin camı arasındaki sınır, girintili yani sıcaklık düştükçe ferromanyetik faza doğru kayan veya çıkık yani sıcaklık düştükçe spin camı fazına doğru ilerleyen özelliğe sahiptir. Ancak bu sınır eğer Nishimori simetri çizgisiyle kesişen bir çoklu kritik nokta ile sonlanıyorsa her zaman girintili davranış göstermektedir.

ACKNOWLEDGMENTS

I would like to thank my advisor Prof. A. Nihat Berker for his guidance, imbuing me with enthusiasm for research, continuously contributing to my research progress for more than three years, and sharing his understanding of perfection. I also want to thank Dr. Michael Hinczewski for being such an extraordinary co-advisor, answering all my questions starting from fundamental facts, having lovely after-lunch talks with me for six months, and enhancing my numerical techniques. In addition, I thank Prof. Hidetoshi Nishimori for being helpful and kind, and also my parents and Serap Süvari for their compassion and support.

TABLE OF CONTENTS

LIST OF TABLES

LIST OF FIGURES

Chapter 1

INTRODUCTION

1.1 Types of Phase Transitions

Phase transitions are signalled by the singularities in the order parameter or in the response functions. Focusing on the phase diagram of carbon dioxide (Figure 1.1), we see three phases coexisting at point T, known as the triple point, or each of them coexisting with one of the others along the lines. These lines are first-order phase transition boundaries.

In this particular case the order parameter is the density. The phase boundary dividing the liquid and the solid phases extends to infinity. The reason for that is the occurrence of a symmetry breaking. In the solid phase there is a frozen density wave having a non-zero amplitude, while the liquid phase has translational symmetry. In other words the result of the density operator, which counts the particles in a small volume, does not change by translating its argument x by any deviation.

However in the solid phase there is an "atom-no atom" construction. Because of this the two phases will coexist along the solid-liquid phase boundary and there will always be a discontinuity in the order parameter. The phase boundary between gaseous and liquid states is terminated by a critical point. At this point there is no coexistence of different states, but still there is phase transition, which is called a second-order phase transition. Unlike the first-order transition, in a second-order transition, large and long-lived fluctuations are observed. Moreover, the correlation length becomes infinite, which causes singularities in response functions.

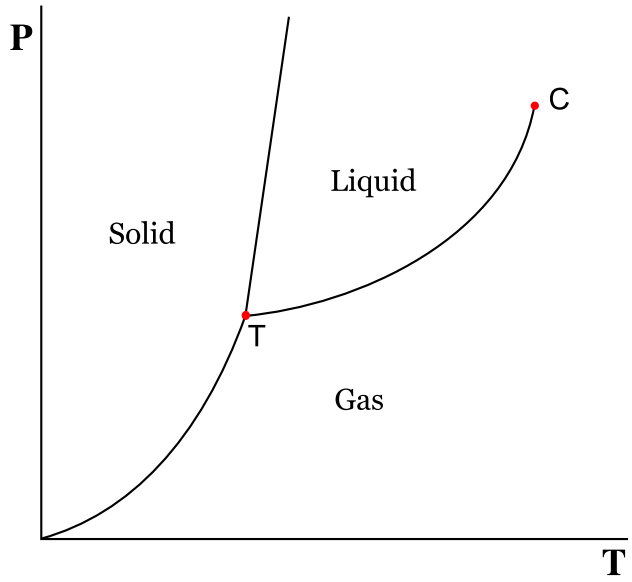

Figure 1.1: Phase diagram of carbon dioxide.

1.1.1 Critical Behavior

The singularities in the response functions obey power laws, and the exponents that define the critical behavior of these singularities are called critical exponents. These exponents are classified as given in Table 1.1.

1.1.2 Example: Specific Heat

Internal energy is the thermodynamic average of the Hamiltonian.

$$U =< \mathcal{H} >= \frac{\mathbf{Tr}\ \mathcal{H}e^{-\beta\mathcal{H}}}{\mathbf{Tr}\ e^{-\beta\mathcal{H}}} = -\frac{\mathbf{Tr}\ \frac{\partial}{\partial\beta}e^{-\beta\mathcal{H}}}{\mathbf{Tr}\ e^{-\beta\mathcal{H}}}\,, \tag{1.1}$$

where the trace **Tr** denotes a sum over all the states of the system. Specific heat is given by

$$C = \frac{\partial U}{\partial T} = \frac{\partial U}{\partial \beta}\frac{\partial \beta}{\partial T} = -k_B\beta^2\frac{\partial U}{\partial \beta}\,. \tag{1.2}$$

Substituting (1.1) into (1.2) results in

$$C = k_B\beta^2\left(\frac{\mathbf{Tr}\ \frac{\partial^2 e^{-\beta\mathcal{H}}}{\partial\beta^2}}{\mathcal{Z}} - \left(\frac{\mathbf{Tr}\ \frac{\partial e^{-\beta\mathcal{H}}}{\partial\beta}}{\mathcal{Z}}\right)^2\right)\,. \tag{1.3}$$

Note that $\mathbf{Tr}\ e^{-\beta\mathcal{H}} = \mathcal{Z}$, and $J = \beta\tilde{J}$, $\frac{\partial}{\partial\beta} = \frac{\partial J}{\partial\beta}\frac{\partial}{\partial J} = \tilde{J}\frac{\partial}{\partial J}$. Using this, equation (1.3) reduces to

Physical property	Behavior	Notes
Specific Heat	$C = dU/dT \sim \|t\|^{-\alpha}$	$\alpha > 0$: divergence $\alpha < 0$: cusp
Correlation length	$\xi \sim \|t\|^{-\nu}$	$\nu > 0$
Critical correlation function	$\Gamma(r) \sim \frac{1}{r^{d-2+\eta}}$	$\eta \geq 0$
Compressibility	$\kappa = -\frac{1}{V}\frac{\partial V}{\partial P} \sim \|t\|^{-\gamma}$	$\gamma > 0$
Density	$(\rho_L - \rho_G) \sim t^{\beta}$	$\beta > 0$
Susceptibility	$\chi = \partial M/\partial H \sim \|t\|^{-\gamma}$	
Magnetization	$M \sim t^{\beta}$	

Table 1.1: Power law behaviors of order parameters and response functions at the critical point.

$$
\begin{aligned}
C &= k_B\beta^2\tilde{J}^2\left(\frac{\mathbf{Tr}\ \left(\sum_{<ij>} s_i s_j\right)\left(\sum_{<kl>} s_k s_l\right) e^{-\beta\mathcal{H}}}{\mathcal{Z}} - \left(\frac{\mathbf{Tr}\ \sum_{<ij>} s_i s_j}{\mathcal{Z}}\right)\left(\frac{\mathbf{Tr}\ \sum_{<kl>} s_k s_l}{\mathcal{Z}}\right)\right) \\
&= k_B J^2\left(\sum_{<ij>,<kl>} < s_i s_j s_k s_l > - \left(\sum_{<ij>} < s_i s_j >\right)\left(\sum_{<kl>} < s_k s_l >\right)\right) \\
&= k_B J^2 \sum_{<ij>,<kl>} < s_i s_j s_k s_l > - < s_i s_j >< s_k s_l > \\
&= k_B J^2 \sum_{<ij>,<kl>} \Gamma(\vec{r}_{ij}, \vec{r}_{kl}) \qquad (1.4) \\
&= \frac{Nq}{2} k_B J^2 \sum_{<ij>} \tilde{\Gamma}(\vec{r}_{ij})\,. \qquad (1.5)
\end{aligned}
$$

Equation (1.5) constitutes "specific heat sum rule". This summation can be converted into an integral, with lattice spacing a and system length L. The behavior of the specific heat can be investigated at criticality as well as near the critical point. We define $r \equiv |\vec{r}_i - \vec{r}_j|$.

I. At criticality, since $\xi \to \infty$, the specific heat per particle becomes,

$$\frac{C}{N} \sim \int_a^L r^{d-1} dr \frac{1}{r^u}\,. \qquad (1.6)$$

Let $x \equiv r/L$,

$$\frac{C}{N} \sim L^{d-u} \int_{a/L \to 0}^{1} x^{d-1-u} dx \,. \tag{1.7}$$

Letting, $u \equiv d - 2 + \eta_T$, and we can write:

$$\frac{C}{N} \sim L^{2-\eta_T} \int_{0}^{1} x^{1-\eta_T} dx \,. \tag{1.8}$$

Therefore in thermodynamic limit, $L \to \infty$, there is a singularity in the specific heat per particle for $\eta_T < 2$.

II. Near the critical point the greatest contribution to the integral will come from the interval $r = [a, \xi]$:

$$\begin{aligned} \frac{C}{N} &\sim \int_{a}^{\xi} r^{1-\eta_T} dr e^{-r/\xi} \\ &\sim \int_{a}^{\xi} r^{1-\eta_T} dr \\ &\sim \xi^{2-\eta_T} \,. \end{aligned} \tag{1.9}$$

Finally, using equation (1.9) and the power laws from Table 1.1, the relation between α, ν and η_T is obtained: $\alpha = (2 - \eta_T)\nu$.

1.2 Universality

It has been observed that the values of the critical exponents are the same even if they are measured for different systems. This phenomenon was discovered a long time before physicists began their efforts to explain critical phenomena. As an example, the critical exponents for the $YFeO_3$ ferromagnet, CO_2 and Xe fluids, the FeF_2 antiferromagnet, beta-brass alloy, the NH_4Cl molecular crystal and the $d = 3$ Ising model in any lattice are the same. These systems form a universality class. Another universality class consists of XY-magnets, superfluid helium, and liquid crystals, which have the same numerical values for the critical exponents. In other words they share the same critical properties, which are different from the previously mentioned universality class. Therefore a theory which describes critical phenomena should also explain the principle of universality.

1.3 History

The evolution of physical theories of phase transitions can be summarized historically. Until 1960 critical phenomena was explained using different forms of mean-field-theory: Curie-Weiss, molecular field, Hartree, Landau and Gibbs theories. Between 1960 and 1970, high-order perturbation theory and molecular dynamics were developed, along with Monte Carlo simulations and droplet theories. L. P. Kadanoff' s scaling theory in 1966 marked a turning point in that era. In 1971 K.G. Wilson introduced renormalization-group theory which was a significant advance in statistical and particle physics. This approach was applied in a variety of fields. The chronological order is as follows:

* 1980' s neural networks, quenched disorder, spin glasses

* 1990' s economics, markets, earthquakes

* 2000' s small-world-networks, quantum systems

Chapter 2

RENORMALIZATION-GROUP APPROACH

2.1 Scaling Theory of Kadanoff

The basic idea of Kadanoff' s scaling theory is coarse graining. Spins are grouped in cells, with each cell containing b^d spins. The *rescaled* variable $s'_{i'}$ carries the collective property of all spins inside its block. The assumption is that the physics governing the original system does not change after the rescaling transformation. By doing consecutive rescalings, it can be seen that some quantities are amplified, known as relevant fields, while others are supressed, known as irrelevant fields. The distinction between relevant and irrelevant fields depends on macroscopic quantities.

2.1.1 Example: Ising ferromagnet

The Ising ferromagnet has the Hamiltonian

$$-\beta\mathcal{H} = J\sum_{\langle ij\rangle} s_i s_j + H\sum_i s_i \,. \tag{2.1}$$

The cell variable is defined as

$$s'_{i'} = b^{-d}\sum_{i}^{i'} s_i \,. \tag{2.2}$$

Since the physics is not modified after the transformation, in order to conserve the structure of the problem the cell variable should be written in the form

$$s'_{i'} = \mathrm{sgn}\left(\sum_{i}^{i'} s_i\right) . \tag{2.3}$$

The original system has N spins with lattice spacing a, while the rescaled system has $N' = N/b^d$ sites with a rescaled spacing $a' = ba$. The two systems can be made equivalent by the appropriate choice of J' as well as H'. Thus the partition function is not changed but it is a function of the rescaled variables:

$$\mathcal{Z}(t, H) = \mathcal{Z}(t', H')\,, \tag{2.4}$$

where $t \equiv \dfrac{J_c - J}{J_c}$. The rescaled interactions are assumed to be analytic functions of the original physical quantities. The relations between the original and rescaled interactions are called recursion relations, and can be written as:

$$t' = t'(t, H)\,, \tag{2.5}$$

$$H' = H'(t, H)\,. \tag{2.6}$$

Because of analyticity these functions can be linearized around the critical point, and with interchange of up and down directions (i.e. $s \to -s$, $H \to -H$, $t \to t$ and the same mappings for the primed variables) the recursion relations near critical point become:

$$t' = b^{y_T} t \quad \text{and} \quad H' = b^{y_H} H\,. \tag{2.7}$$

Instead of b^{y_T} and b^{y_H} anything else can be chosen but this mapping satisfies two group properties, closure and existence of the identity, making the rescaling transformation a semi-group.

Dimensionless Free Energy

We start with Eq. (2.4), and take the logarithm of both sides,

$$\ln \mathcal{Z} = \ln \mathcal{Z}'\,, \tag{2.8}$$

$$N f(t, H) = N' f(t', H')\,, \tag{2.9}$$

$$f(t, H) = b^{-d} f(b^{y_T} t, b^{y_H} H)\,. \tag{2.10}$$

By choosing $b = t^{-1/y_T}$ the free energy per particle reduces to

$$f(t, H) = t^{d/y_T} f\left(1, \frac{H}{t^{y_H/y_T}}\right) \tag{2.11}$$

$$= t^{d/y_T}\,\mathrm{func}\left(\frac{H}{t^{y_H/y_T}}\right)\,. \tag{2.12}$$

The specific heat is proportional to the second derivative of the free energy, and from Table 1.1 it scales with $t^{-\alpha}$. Therefore approaching the critical point from the thermal direction, the value for α can be deduced,

$$\alpha = \frac{d}{y_T} - 2\,. \tag{2.13}$$

On the other hand, to approach the critical point from the symmetry-breaking direction b has to have the form $b = H^{-1/y_H}$. Therefore, the scaling form becomes

$$f(t, H) = H^{d/y_H}\,\text{func}\left(1, \frac{t}{H^{y_T/y_H}}\right)\,. \tag{2.14}$$

The magnetization is defined as the magnetic field derivative of the free energy, $M = \dfrac{\partial f}{\partial H}$, and it is bounded ($|M| \leq 1$). As $H \to 0$ the magnetization does not diverge if $\dfrac{d}{y_H} \geq 1$. The nearest-neighbor correlations are related to the t derivative of the free energy, $\langle s_i s_j \rangle \sim \dfrac{\partial f}{\partial t}$. From Eq. (2.12) it can be seen that $\dfrac{d}{y_T} \geq 1$. Overall, the critical exponents are bounded by zero from below, because they describe relevant fields, and from the above analysis their upper limit is d,

$$y_H, y_T \in [0, d]\,. \tag{2.15}$$

As can be seen, a simple examination of the free energy yields a large amount of information about critical behavior and critical exponents, giving a very good demonstration of the theory.

Correlation Length at $H = 0$

Correlation length scales with exponent ν near the critical point, $\xi = \xi_0 t^{-\nu}$. By substituting in the rescaled temperature one finds

$$\begin{aligned} \xi' &= \xi_0 t'^{-\nu} \\ &= \xi_0 (b^{y_T} t)^{-\nu} \\ &= b^{-y_T \nu} \xi\,. \end{aligned} \tag{2.16}$$

Because of length rescaling, $\xi' = b^{-1}\xi$. Comparison of this relation with Eq. (2.16) results in $\nu = \dfrac{1}{y_T}$. This result can be used in Eq. (2.13) to get a hyperscaling relation,

$$2 - \alpha = d\nu \,. \tag{2.17}$$

Magnetization

Magnetization is the H derivative of the free energy per particle

$$M(t, H) = \frac{1}{N}\frac{\partial}{\partial H} \ln \mathcal{Z}(t, H) \,. \tag{2.18}$$

By substituting the rescaled variables into Eq. (2.18) one obtains

$$\begin{aligned} M(t, H) &= \frac{b^{-d}}{N'} b^{y_H} \frac{\partial}{\partial H'} \ln \mathcal{Z}'(t', H') \\ &= b^{y_H - d} \frac{1}{N'} \frac{\partial}{\partial H'} \ln \mathcal{Z}' \\ &= b^{y_H - d} M(t', H') \,. \end{aligned} \tag{2.19}$$

To approach from the thermal direction, the appropriate choice of b is, $b = t^{-1/y_T}$. Then Eq. (2.19) becomes,

$$\begin{aligned} M &= t^{(d-y_H)/y_T} M\left(1, \frac{H}{t^{y_H/y_T}}\right) \\ &= t^{(d-y_H)/y_T} \text{func}\left(\frac{H}{t^{y_H/y_T}}\right) \,. \end{aligned} \tag{2.20}$$

To find the critical behavior of magnetization with respect to temperature, one needs to move along thermal direction, $H = 0$, giving the critical exponent β,

$$\begin{aligned} M(t) &\sim t^{(d-y_H)/y_T} \,, \\ \beta &= \frac{d - y_H}{y_T} \,. \end{aligned} \tag{2.21}$$

To approach the critical point along the magnetic field direction the appropriate choice of b is: $b = H^{-1/y_H}$. Plugging that into Eq. (2.19) one obtains the scaling form of the magnetization with respect to magnetic field,

$$M(t,H) = H^{(d-y_H)/y_H}\,\mathrm{func}\left(\frac{t}{H^{y_T/y_H}}\right). \tag{2.22}$$

At $t = 0$, the relation for the critical exponent δ is obtained,

$$\delta = \frac{d}{y_H} - 1\,. \tag{2.23}$$

Correlation Function

For a local field, which affects only one spin, the recursion relation becomes,

$$H'_{i'} = \frac{b^{y_H}}{b^d} H_i\,. \tag{2.24}$$

The two-point correlation function is a measure of the correlation of spin pairs separated by a distance r,

$$\begin{aligned} \Gamma(r,t,H) &= \langle s_0 s_r\rangle - \langle s_0\rangle\langle s_r\rangle \\ &= \frac{\partial^2}{\partial H_0 \partial H_r} \ln \mathcal{Z} \\ &= b^{2y_H-d}\Gamma(b^{-1}r, b^{y_T}t, b^{y_H}H)\,. \end{aligned} \tag{2.25}$$

By choosing $b = r$, it reduces to

$$\Gamma(r,t,H) = \frac{\mathrm{func}(r^{y_T}t, r^{y_H}H)}{r^{2(d-y_H)}}\,. \tag{2.26}$$

At the critical point, the general behavior of the correlation function is obtained, and the critical exponent η can be deduced as a function of the scaling exponents,

$$\begin{aligned} \Gamma(r,t=0,H=0) &= \frac{A}{r^{2(d-y_H)}} \\ &\Rightarrow\quad d-2+\eta = 2d-2y_H\,, \\ \eta &= d+2-2y_H\,. \end{aligned} \tag{2.27}$$

2.1.2 Results

From the analysis it can be seen that the scaling exponents determine all the critical exponents. Furthermore, the scaling exponents relate critical exponents to each other. Given the simplicity of the technique the amount of information that has been acquired is impressive. However, other physical quantities away from the critical temperature cannot be calculated using the recursion relations from Kadanoff's theory. Also, the theory assumes the analyticity of the recursion relations, but no explicit forms of the relations could be derived. The two negative aspects are related, but the renormalization-group theory described in the next section has solutions to both of them.

2.2 Renormalization-Group Theory

In contrast to Kadanoff's theory the recursion relations can be calculated in renormalization-group theory. Instead of focusing on the critical point, the renormalization-group analysis starts from calculating the partition function, with the same requirement of its invariance under rescaling,

$$\begin{aligned} \mathcal{Z} &= \sum_{\{s\}} e^{-\beta\mathcal{H}} \\ &= \sum_{\{s'\}} \left(\sum_{\{\sigma\}} e^{-\beta'\mathcal{H}'(\{s'\},\{\sigma\})} \right) \\ &= \sum_{\{s'\}} e^{-\beta'\mathcal{H}'(\{s'\})} \\ &= \mathcal{Z}' \end{aligned}$$

With this operation, the recursion relations that connect the rescaled system to the original system can be obtained as analytic functions. The renormalized Hamiltonian $\mathcal{H}'$ may have a more general form than the original Hamiltonian. Considering the Ising ferromagnet Eq. (2.1) as example, an extra term will be produced by the renormalization-group transformation, which is called the additive constant. It plays an important role in the calculation of the free energy. The renormalization-group flows describe a bigger picture

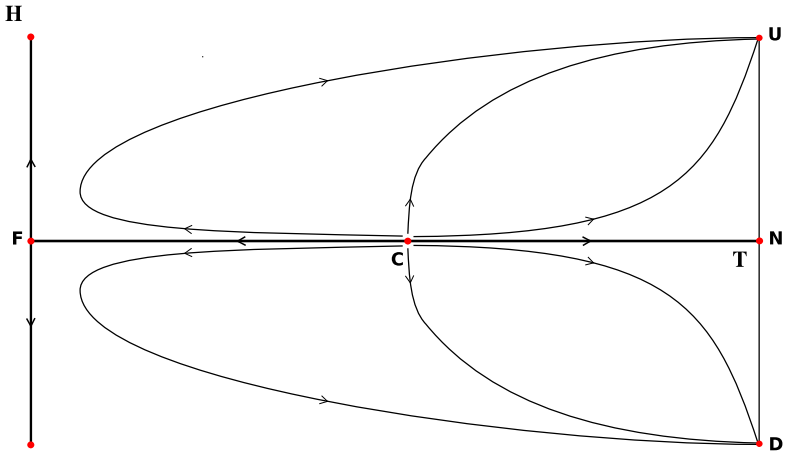

Figure 2.1: Renormalization-group flows of the Ising ferromagnet in two dimensions.

than the Kadanoff picture, and also give detailed information about thermodynamic fields in the whole phase space.

The linearization of the recursion relations about a non-trivial critical point produces information about critical exponents. In the flow space the flows are controlled by fixed points, classified as trivial and non-trivial fixed points depending on the behavior of the correlation length. At a trivial fixed point the correlation length is zero, while it diverges to infinity at a non-trivial point. In Figure 2.1 points other than the critical point are trivial fixed points. F controls the first-order transition, U and D are up and down sinks and N controls the flow on the temperature axis for values of T greater than the critical temperature.

In addition to that, thermodynamic functions can be calculated using the renormalization-group flows, by constructing a recursion matrix T with elements:

$$T_{\beta\alpha} = \frac{q_\beta}{q_\alpha} \frac{\partial K'_\beta}{\partial K'_\alpha} , \tag{2.28}$$

where K_α , $\alpha = 1, \ldots ,m$, denotes the m interaction parameters in the Hamiltonian. The density that corresponds to K_α can be calculated using renormalization-group flows,

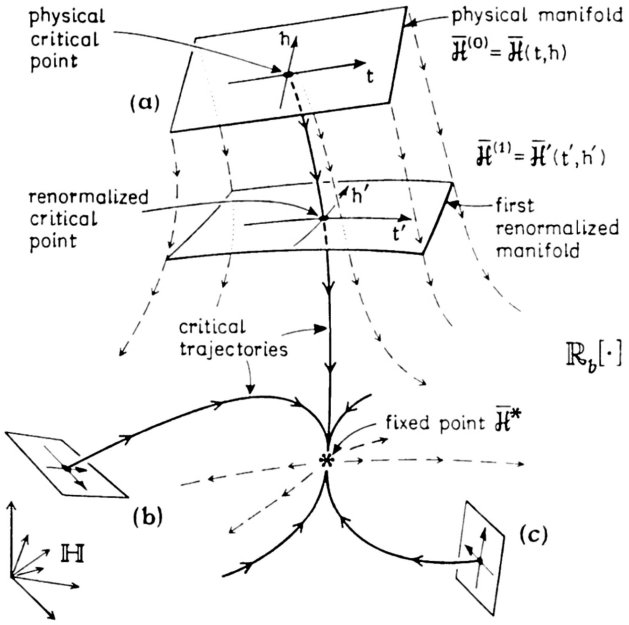

Figure 2.2: Renormalization-group flows of different physical manifolds (a), (b) and (c) [1].

$$
\begin{aligned}
M_\alpha &= \frac{1}{N_\alpha}\frac{\partial}{\partial K_\alpha}\ln \mathcal{Z} \\
&= \frac{b^{-d}}{q_\alpha N'}\frac{q_\beta}{q_\beta}\sum_\beta \frac{\partial K'_\beta}{\partial K_\alpha}\frac{\partial \ln \mathcal{Z}}{\partial K'_\beta} \\
&= b^{-d}\sum_\beta M'_\beta \frac{q_\beta}{q_\alpha}\frac{\partial K'_\beta}{\partial K_\alpha} \\
&= b^{-d}\sum_\beta M'_\beta T_{\beta\alpha}\,, \qquad (2.29)
\end{aligned}
$$

The renormalization-group picture gives an explanation of the concept of universality Section 1.2. The flows show, why different Hamiltonians have the same exponents. In the Figure 2.2, a fixed point controls different Hamiltonians of the same universality class. The critical points of each physical manifold all flow to a single fixed point.

2.3 Spin Glasses

A spin glass consists of randomly oriented spins with their orientation frozen in time [2]. In other words, the magnetization is zero if it is averaged over space, however, the time average of a single spin is non-zero. To distinguish the spin-glass and paramagnetic phases, since in both phases the magnetization is zero, it is convenient to define a spin-glass parameter q. Before defining m and q, one needs to introduce the configurational average.

For an Ising spin glass the microscopic interactions are described by the Hamiltonian:

$$\mathcal{H} = -\sum_{\langle ij \rangle} J_{ij} s_i s_j, \quad s_i = \pm 1 \tag{2.30}$$

The interactions J_{ij} are randomly distributed throughout the system, with the probability distributions typically assumed to be Gaussian or $\pm J$,

$$\text{Gaussian:} \quad P(J_{ij}) = \frac{1}{\sqrt{2\pi J^2}} \exp\left(-\frac{(J_{ij}-J_0)^2}{2J^2}\right), \tag{2.31}$$

$$\pm \text{ J}: \quad P(J_{ij}) = p\delta(J_{ij}+J) + (1-p)\delta(J_{ij}-J). \tag{2.32}$$

These distributions describe the quenched (fixed) distribution of bonds in a system. The configurational average is calculated over all possible distributions of bonds in the system. It is denoted by brackets [...], and has the explicit form

$$[A] = \int \prod_{\langle ij \rangle} dJ_{ij} P(J_{ij}) A, \tag{2.33}$$

where A represents a physical quantity. The local magnetization, which is the thermodynamic average of a spin at site i, has the form

$$m_i = \frac{\mathbf{Tr}\ s_i e^{-\beta\mathcal{H}}}{\mathbf{Tr}\ e^{-\beta\mathcal{H}}}. \tag{2.34}$$

The magnetization m is the configurational average of the local magnetization, $m = [m_i]$. As stated above, to distinguish spin-glass and paramagnetic behaviors it is important to introduce a spin glass order parameter $q = [\langle s_i \rangle^2]$. In a paramagnet m and q are zero. In the spin-glass phase though m is zero, q is greater than zero. There are many bond configurations corresponding to the same bond distribution. In a spin glass if m_i is averaged

over one configuration, it may have a positive value, while another average over a different configuration may result in a negative value. Eventually the average over all configurations results in $m = 0$. However, the square of the average is always positive, therefore if it is averaged over different configurations it will be positive.

2.3.1 Nishimori Symmetry

The Hamiltonian given in Eq. (2.30) can be gauge transformed by the following maps:

$$s_i \to s_i\sigma_i \quad , \quad J_{ij} \to J_{ij}\sigma_i\sigma_j \,, \tag{2.35}$$

where $\sigma_i \in \{-1, 1\}$ and is independent of s_i. The internal energy is the thermodynamic average of $\mathcal{H}$ and its configurational average is,

$$\begin{aligned} [E] &= \left[\frac{\mathbf{Tr}\ \mathcal{H}e^{-\beta\mathcal{H}}}{\mathbf{Tr}\ e^{-\beta\mathcal{H}}}\right] \\ &= \int \prod_{\langle ij\rangle} dJ_{ij} P(J_{ij}) \frac{\mathbf{Tr}\ \left(-\sum_{\langle ij\rangle} J_{ij}s_is_j\right) e^{\beta\sum_{\langle ij\rangle} J_{ij}s_is_j}}{\mathbf{Tr}\ e^{\beta\sum_{\langle ij\rangle} J_{ij}s_is_j}} \,. \end{aligned} \tag{2.36}$$

Since the Hamiltonian $\mathcal{H}$ is invariant under the gauge transformation, we can apply the transformations shown in Eq. (2.35) in Eq. (2.36)

$$\begin{aligned} [E] &= \int \prod_{\langle ij\rangle} dJ_{ij} P(J_{ij}\sigma_i\sigma_j) \frac{\mathbf{Tr}\ \left(-\sum_{\langle ij\rangle} J_{ij}s_is_j\sigma_i^2\sigma_j^2\right) e^{\beta\sum_{\langle ij\rangle} J_{ij}s_is_j\sigma_i^2\sigma_j^2}}{\mathbf{Tr}\ e^{\beta\sum_{\langle ij\rangle} J_{ij}s_is_j\sigma_i^2\sigma_j^2}} \\ &= \int \prod_{\langle ij\rangle} dJ_{ij} P(J_{ij}\sigma_i\sigma_j) \frac{\mathbf{Tr}\ \left(-\sum_{\langle ij\rangle} J_{ij}s_is_j\right) e^{\beta\sum_{\langle ij\rangle} J_{ij}s_is_j}}{\mathbf{Tr}\ e^{\beta\sum_{\langle ij\rangle} J_{ij}s_is_j}} \,. \end{aligned} \tag{2.37}$$

Note that we have used $\sigma_i^2 = 1$ and $\left|\prod_{\langle ij\rangle}\sigma_i\sigma_j\right| = 1$, which is the Jacobian of the transformed variables. We assume $P(J_{ij}\sigma_i\sigma_j)$ has the form

$$\tilde{P}(|J_{ij}\sigma_i\sigma_j|)e^{aJ_{ij}\sigma_i\sigma_j} \,. \tag{2.38}$$

In addition to that, since the RHS of the equation does not depend on the gauge variables σ specifically, we can sum the RHS of the equation over all possible configurations of σ and

divide that by the total number of configurations, which is 2^N. Thus, the configurational average of the internal energy becomes:

$$[E] = \frac{1}{2^N} \int \left(\prod_{\langle ij \rangle} dJ_{ij} \tilde{P}(|J_{ij}|) \right) \mathbf{tr}\ e^{a \sum_{\langle ij \rangle} J_{ij} \sigma_i \sigma_j} \frac{\mathbf{Tr}\ \left(- \sum_{\langle ij \rangle} J_{ij} s_i s_j \right) e^{\beta \sum_{\langle ij \rangle} J_{ij} s_i s_j}}{\mathbf{Tr}\ e^{\beta \sum_{\langle ij \rangle} J_{ij} s_i s_j}}, \tag{2.39}$$

with **tr** being the trace over the set $\{\sigma\}$. If $a = \beta$ then the denominator and the trace over σ are equal to the partition function of the same configuration and they cancel each other. The condition $a = \beta$ defines the *Nishimori line*. The expression becomes

$$\begin{aligned}
[E] &= \frac{1}{2^N} \int \left(\prod_{\langle ij \rangle} dJ_{ij} \tilde{P}(|J_{ij}|) \right) \mathbf{Tr}\ \left(- \sum_{\langle ij \rangle} J_{ij} s_i s_j \right) e^{\beta \sum_{\langle ij \rangle} J_{ij} s_i s_j} \\
&= \frac{1}{2^N} \int \left(\prod_{\langle ij \rangle} dJ_{ij} \tilde{P}(|J_{ij}|) \right) \mathbf{Tr}\ \left(- \frac{\partial}{\partial \beta} \right) e^{\beta \sum_{\langle ij \rangle} J_{ij} s_i s_j} \\
&= -\frac{1}{2^N} \frac{\partial}{\partial \beta} \mathbf{Tr}\ \left(\prod_{\langle ij \rangle} \int dJ_{ij} \tilde{P}(|J_{ij}|) e^{\beta J_{ij} s_i s_j} \right) \\
&= -\frac{1}{2^N} \frac{\partial}{\partial \beta} \mathbf{Tr}\ \left(\int dJ \tilde{P}(J) e^{\beta J} \right)^{N_B} \\
&= -\frac{\partial}{\partial \beta} \left(\int dJ \tilde{P}(J) e^{\beta J} \right)^{N_B}.
\end{aligned} \tag{2.40}$$

2.3.2 Nishimori Line for the ± J Model

We define the variable $\tau_{ij} \equiv J_{ij}/J$, so the $\pm J$ distribution in Eq. (2.32) can be rewritten as

$$P(J_{ij}) = \frac{e^{\kappa_p}}{2 \cosh \kappa_p} (\delta(\tau_{ij} + 1) + \delta(\tau_{ij} - 1)), \tag{2.41}$$

where $e^{2\kappa_p} \equiv \dfrac{1-p}{p}$. Equation (2.41) has the same form in Eq. (2.38) with $a = \dfrac{\kappa_p}{J}$. Finally, the Nishimori line for $\pm J$ model is obtained through, $aJ = \beta J = \kappa_p$ or, $e^{2\beta J} = \dfrac{1-p}{p}$. The Nishimori line is a subspace, which is closed under the renormalization-group transformation. Therefore the probability distributions, evolving with consecutive renormalization-group transformations have to satisfy the Nishimori symmetry at each step. In a phase diagram, for which the Nishimori condition is satisfied on a line, the point that intersects

the Nishimori line is a special point and if there exists a multicritical point in that phase diagram one expects the two special points to be the same.

Chapter 3

REENTRANT AND FORWARD PHASE DIAGRAMS OF THE ANISOTROPIC $d = 3$ ISING SPIN-GLASS

3.1 Introduction

The Ising spin glass [2] yields a phase diagram with a distinctively complex ordered phase, in $d = 3$. A wide accumulation of methods and results has occurred for this system. Most remarkably, in spite of its high spatial dimension and complex ordering behavior, exact information is being obtained for this system.[3, 4, 5, 7, 6, 8, 9, 10, 11, 12, 13] Thus, in the phase diagram in terms of temperature and concentration of antiferromagnetic bonds, the occurrence of the Nishimori symmetry line [3, 4] and the exact location of the multicritical point [11, 13] have been deduced. Furthermore, in systems with the Nishimori symmetry, it has been shown that the ferromagnetic phase cannot extend to antiferromagnetic bond densities beyond that of the multicritical point.[3, 4] The two remaining options being a straight line or a reentrance situation, subsequent works [14, 15] on hierarchical lattices have shown that for these systems, the spin-glass phase diagram is reentrant, namely that below the multicritical point, the ferromagnetic phase recedes from the spin-glass phase as temperature is lowered. Exact results recently have also been extended to Potts spin glasses.[16]

A spatially uniaxially anisotropic $d = 3$ system is studied in this work, to our knowledge the first study of quenched randomness and frustration in a spatially anisotropic higher-dimensional system. In fact, both anisotropy and quenched randomness have acquired increased relevance from high-temperature superconductivity results.[17, 18] Our calculation is exact for a hierarchical lattice and approximate for a tetragonal lattice. We find a rich phase diagram (e.g., Fig.3.1) with five different ordered phases, namely with ferromagnetic, antiferromagnetic, layered, columnar, and spin-glass order. The spin-glass phase is more extensive when randomness is introduced within the planes than when it is introduced in

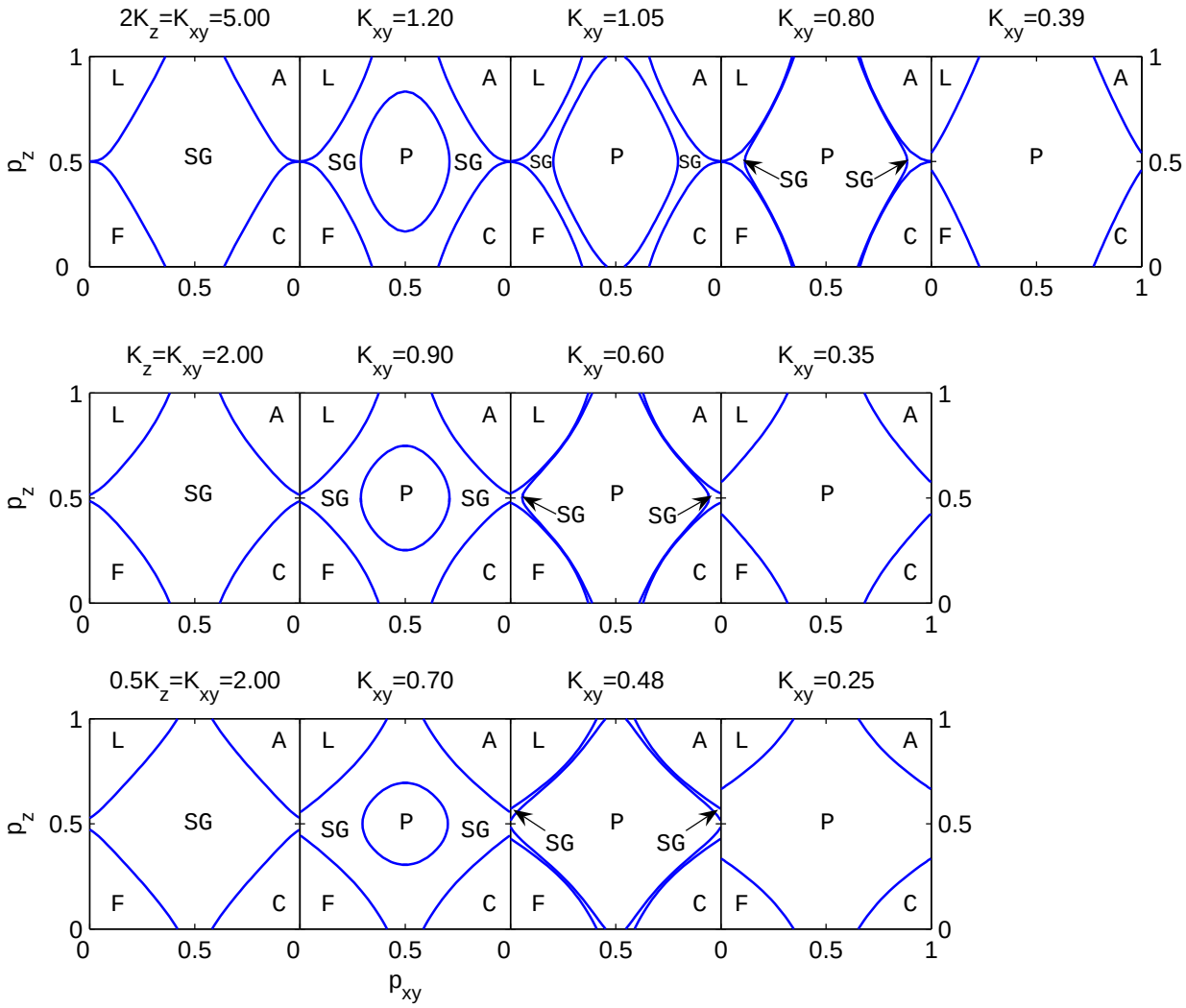

Figure 3.1: Top line: Constant-temperature cross-sections of the global phase diagram for $K^z/K^{xy} = 0.5$, as a function of p_{xy} and p_z, which are the concentrations of antiferromagnetic xy and z bonds, respectively. At low temperatures (high K^{xy}), the central spin-glass (SG) phase separates the corner ferromagnetic (F), columnar (C), antiferromagnetic (A), and layered (L) phases. The diagrams are twofold symmetric along each axis, but not fourfold symmetric, due to the difference between longitudinal ($p_{xy} = 0$) and transverse ($p_z = 0$) spin glasses. As temperature increases, the paramagnetic (P) phase appears at the central point, first reaches the transverse spin-glass system and eliminates the spin-glass phase, then reaches the longitudinal spin-glass system and eliminates the spin-glass phase. In the latter system, the spin-glass and paramagnetic phases simultaneously occur for a very narrow range of temperatures, as also seen in the inset in the lower left panel of Fig. 3.3 Middle line: Constant-temperature cross-sections for $K^z = K^{xy}$. Bottom line: Constant-temperature cross-sections for $K^z/K^{xy} = 2$. All phase transitions in this figure are second order.

lines along one direction.

The global phase diagram includes cross-sections with no Nishimori symmetry, cross-sections with Nishimori symmetry lines, and a cross-section entirely imbedded within Nishimori symmetry. Thus, the multicritical point between the spin-glass, ferromagnetic, and paramagnetic phases, previously found to occur on the Nishimori symmetry line, is also found here at points with no Nishimori symmetry, but renormalizes to a fixed distribution of interaction probabilities that obeys Nishimori symmetry. Nevertheless, we find that the boundary between the ferromagnetic and spin-glass phases can be either reentrant or forward, that is either receding from or penetrating into the spin-glass phase, as temperature is lowered. When the multicitical point is not on the Nishimori symmetry line, the ferromagnetic-spin glass boundary can be reentrant or forward. When the multicritical point is on the Nishimori symmetry line, this boundary is always reentrant [14, 15], consistently with the rigorous result [3, 4].

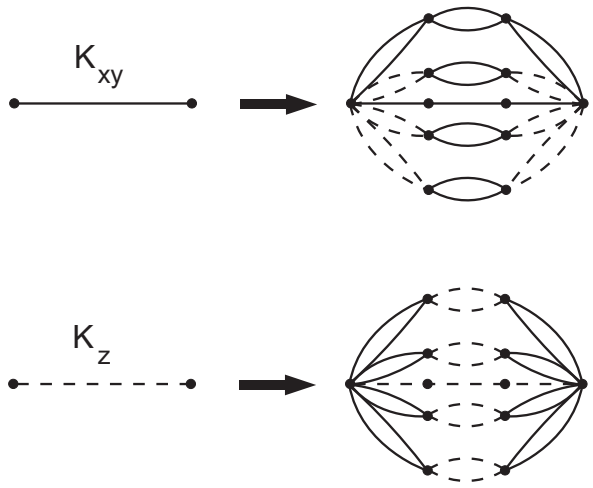

Figure 3.2: Construction of the uniaxially anisotropic d=3 hierarchical model. Two graphs are mutually and repeatedly self-imbedded. Note that for $K^{xy} = 0, K^z = 0$, and $K^{xy} = K^z$, the system reduces respectively to the $d = 1$, isotropic $d = 2$ and $d = 3$ systems.

3.2 Uniaxially Anisotropic Spin Glass

The uniaxially anisotropic Ising spin-glass system has the Hamiltonian

$$-\beta H = \sum_u \sum_{\langle ij \rangle_u} K_{ij}^u s_i s_j \,, \tag{3.1}$$

where $s_i = \pm 1$ at each site i, $\langle ij \rangle_u$ denotes a sum over nearest-neighbor pairs of sites along the z direction ($u = z$) or in the xy plane ($u = xy$), and the bond strengths K_{ij}^u are equal to $K^u > 0$ with probability $1 - p_u$ and $-K^u$ with probability p_u, respectively corresponding to ferromagnetic and antiferromagnetic interaction. When imbedded into a cubic lattice, the Hamiltonian (3.1) yields a uniaxially anisotropic $d = 3$ system.

Hierarchical lattices are d-dimensional lattices yielding exact renormalization-group solutions to complex statistical mechanics problems. These lattices are constructed by the repeated self-imbedding of a graph into a bond [19, 20, 21]. The shortest path between the external vertices of the graph gives the length rescaling factor b and the number of bonds in the graph gives the volume rescaling factor b^d, from which the dimension d is determined. Hierarchical lattices have been used to study a wide variety of problems, including chaotic rescaling [22, 23], spin-glass [14], random-field [24], Schrödinger equation [25], lattice-vibration [26], dynamic scaling [27], random-resistor network [28], aperiodic magnet [29], complex phase diagram [30], directed-path [31], heteropolymer [32], and, most recently, scale-free and small-world network [33, 34, 35, 36, 37, 38, 39, 40] systems, etc. More recently, hierarchical lattices have been created [41] for the study of spatially anisotropic systems. The mutual repeated self-imbedding of two appropriately chosen graphs, with differentiated interactions, yields a uniaxially anisotropic system, whereas a higher number of graphs is needed to achieve higher spatial anisotropy.[41] These hierarchical systems must reduce to isotropy and/or lower spatial dimensions when corresponding interactions are set equal to each other or to zero, as illustrated in Fig.3.1. An anisotropic hierarchical lattice has already been used to obtain the phase diagram of the uniaxially anisotropic $d = 3$ tJ model of electronic conduction.[17] When imbedded into the hierarchical lattice of Fig.3.1, the Hamiltonian (3.1) yields a uniaxially anisotropic $d = 3$ spin-glass system that is exactly soluble.

3.3 Exact Renormalization-Group Solution: Flows of the Quenched Distributions of the Anisotropic Spin-Glass Interactions

The renormalization-group solution proceeds in the direction opposite to the construction of a hierarchical model. Each graph is replaced by a renormalized bond via summation over the spins on the internal sites of the graph. This is achieved by a combination of two types

of steps: the replacement, by a single bond $\widetilde{K}_{ij}$, of two bonds that are either in parallel, referred to as bond-moving:

$$\widetilde{K}_{ij} = K_{ij}^{I} + K_{ij}^{II}\,, \tag{3.2}$$

or in series, referred to as decimation:

$$\widetilde{K}_{ik} = \frac{1}{2}\ln\left[\frac{\cosh(K_{ij}+K_{jk})}{\cosh(K_{ij}-K_{jk})}\right]\,. \tag{3.3}$$

The quenched probability distribution $\widetilde{\mathcal{P}}(\widetilde{K})$ of the replacing bond is calculated by the convolution

$$\widetilde{\mathcal{P}}(\widetilde{K}) = \int dK^{I} dK^{II} \mathcal{P}_{I}(K^{I})\mathcal{P}_{II}(K^{II})\delta(\widetilde{K} - R(K^{I}, K^{II}))\,, \tag{3.4}$$

where $R(K^{I}, K^{II})$ is the right-hand side of Eq.(3.2) or (3.3), K^{I} and K^{II} are the interactions entering the right-hand side of either of these equations, with quenched probability distributions $\mathcal{P}_{I}(K^{I})$ and $\mathcal{P}_{II}(K^{II})$.[24, 14]

Accordingly, the renormalization of $\mathcal{P}_{xy}$ is obtained as follows, following the upper Fig.3.1 in the direction opposite to the arrow: (i) from the bond-moving of $\mathcal{P}_{xy}$ with itself, obtaining $\widetilde{\mathcal{P}}_1$; (ii) from the bond-moving of $\mathcal{P}_z$ with itself, obtaining $\widetilde{\mathcal{P}}_2$; (iii) from the decimation of $\widetilde{\mathcal{P}}_1$ and $\widetilde{\mathcal{P}}_1$, obtaining $\widetilde{\mathcal{P}}_3$; (iv) from the decimation of $\widetilde{\mathcal{P}}_2$ and $\widetilde{\mathcal{P}}_1$, obtaining $\widetilde{\mathcal{P}}_4$; (v) from the decimation of $\mathcal{P}_{xy}$ and $\mathcal{P}_{xy}$, obtaining $\widetilde{\mathcal{P}}_5$; (vi) from the decimation of $\widetilde{\mathcal{P}}_3$ and $\widetilde{\mathcal{P}}_1$, obtaining $\widetilde{\mathcal{P}}_6$; (vii) from the decimation of $\widetilde{\mathcal{P}}_4$ and $\widetilde{\mathcal{P}}_2$, obtaining $\widetilde{\mathcal{P}}_7$; (viii) from the decimation of $\widetilde{\mathcal{P}}_5$ and $\mathcal{P}_{xy}$, obtaining $\widetilde{\mathcal{P}}_8$; (ix) from the bond-moving of $\widetilde{\mathcal{P}}_6$ and $\widetilde{\mathcal{P}}_7$, obtaining $\widetilde{\mathcal{P}}_9$; (x) from the bond-moving of $\widetilde{\mathcal{P}}_7$ and $\widetilde{\mathcal{P}}_7$, obtaining $\widetilde{\mathcal{P}}_{10}$; (xi) from the bond-moving of $\widetilde{\mathcal{P}}_9$ and $\widetilde{\mathcal{P}}_{10}$, obtaining $\widetilde{\mathcal{P}}_{11}$ (xii) finally, from the bond-moving of $\widetilde{\mathcal{P}}_{11}$ and $\widetilde{\mathcal{P}}_8$, obtaining the renormalized quenched distribution $\mathcal{P}'_{xy}$. Thus, in each renormalization-group step, the renormalized distribution $\mathcal{P}'_{xy}$ is obtained from the convolutions of 27 unrenormalized distributions $\mathcal{P}_{xy}$ and $\mathcal{P}_z$. The renormalized distribution $\mathcal{P}'_z$ is similarly obtained from the convolutions of 27 unrenormalized distributions $\mathcal{P}_{xy}$ and $\mathcal{P}_z$, but with a different sequencing dictated by the lower Fig.3.1.

The renormalization-group transformations of the quenched probability distributions $\mathcal{P}_{xy}$ and $\mathcal{P}_z$, given in the preceding paragraph, are implemented numerically, resulting in

Phase	$< K_+^{xy} >$	$< K_-^{xy} >$	$< K_+^{z} >$	$< K_-^{z} >$
Ferro	$+\infty$	0	$+\infty$	0
Antiferro	0	$-\infty$	0	$-\infty$
Columnar	0	$-\infty$	$+\infty$	0
Layered	$+\infty$	0	0	$-\infty$
Spin Glass	$+\infty$	$-\infty$	$+\infty$	$-\infty$
Para	0	0	0	0

Table 3.1: Sinks of the renormalization-group flows in the different phases. These sinks are characterized here in terms of the average positive and negative interactions of their limiting quenched probability distribution.

a distribution of interaction-strength values and a probability associated with each value, namely a histogram. Thus, the initial $\pm K^u$ double-delta distribution functions, described after Eq.(3.1), are of course not conserved under the scale coarsening of the renormalization-group transformation. The number of histograms increases after each convolution. When a maximum number of histograms, set by us, is reached, a binning procedure is applied [24, 14]: Before each convolution, the range of interaction values is divided into bins, separately for positive and negative interactions. The interactions falling into the same bin are combined according to their relative probabilities. The convolution then restores the set maximum number of histograms. In this work, we have used the maximum number of 90,000 for histograms for each distribution $\mathcal{P}_{xy}$ and $\mathcal{P}_z$.

3.4 Phase Diagrams and Fixed Distributions

We have obtained the global phase diagram of the uniaxially anisotropic $d = 3$ spin-glass system in terms of the original interactions and probabilities $(K^{xy}, K^z, p_{xy}, p_z)$. In each thermodynamic phase, quenched probability distributions flow, under repeated renormalization-group transformations, to a limiting behavior (sink) characteristic of that thermodynamic phase. Phase boundary points flow to their own characteristic (unstable) fixed distributions, shown below. Analysis at these unstable fixed distributions yields the order of the phase transitions.[24, 14]

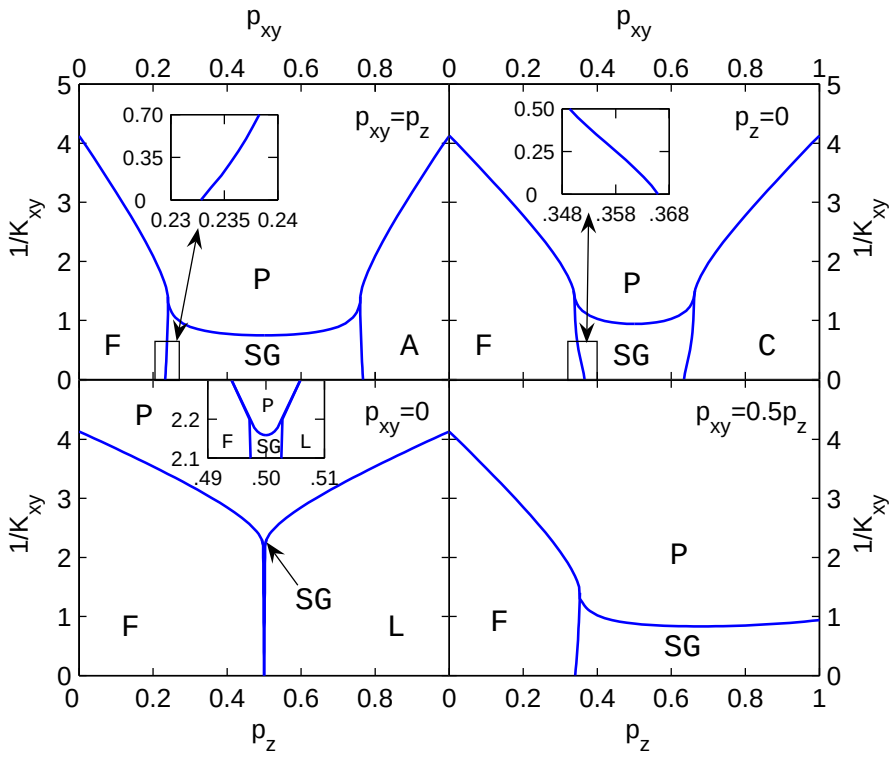

Figure 3.3: Temperature-concentration phase diagrams for isotropically mixed (upper left), transverse (upper right), longitudinal (lower left), and $p_{xy} = 0.5p_z$ spin-glass systems. In all cases, $K^z/K^{xy} = 0.5$. The upper left and right phase diagrams are seen to be, respectively, reentrant and forward, namely with a ferromagnetic phase that, respectively, recedes from or proceeds towards the spin-glass phase as temperature is lowered, as clearly seen in the insets. There are no points obeying Nishimori symmetry in the phase diagrams of this figure. Note the remarkably narrow spin-glass phase, reaching zero-temperature, in the longitudinal spin-glass system, as also seen in the inset. All phase transitions in this figure are second order.

We find six different phases for this system, with corresponding sinks characterized in Table 3.1 in terms of the average positive and negative interactions of the limiting distribution. These phases are the ferromagnetic, antiferromagnetic, layered, columnar, spin-glass ordered phases and the disordered paramagnetic phase. In the layered phase, the spins are mutually aligned in each xy plane; these planes of mutually aligned spins form an antiferromagnetic pattern along the z direction. In the columnar phase, the spins are mutually aligned along the z direction; these lines of mutually aligned spins form an antiferromagnetic pattern along the xy directions. Both of these phases are thus distinct from the antiferromagnetic phase, which is antiferromagnetic in all three directions. There is a single

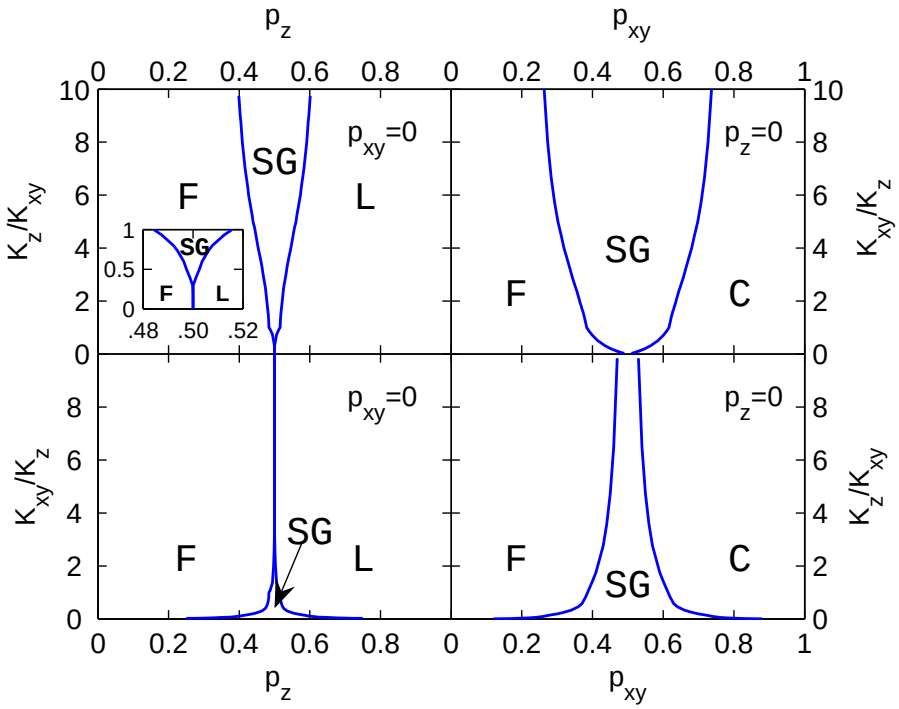

Figure 3.4: Zero-temperature phase diagrams of the longitudinal (left column) and transverse (right column) spin-glass systems. With the appropriate reversal in variables, the transverse and longitudinal spin-glass phase diagrams are seen to be qualitatively similar, but quantitatively different. The spin-glass phase is more extensive in the transverse case. All phase transitions in this figure are second order, shown with blue lines.

spin-glass phase, extending to anisotropic systems.

3.4.1 Phase Diagrams with no Nishimori Symmetry

Cross-sections of the global phase diagram are given in Figs.3.1, 3.3, and 3.4. All phase transitions in these figures are second order. Fig.3.1 shows constant-temperature cross-sections of the global phase diagram as a function of p_{xy} and p_z. At low temperatures (high K^{xy}), the central spin-glass (SG) phase separates the corner ferromagnetic (F), columnar (C), antiferromagnetic (A), and layered (L) phases. The diagrams are twofold symmetric along each axis, but not fourfold symmetric, due to the difference between transverse ($p_z = 0$) and longitudinal ($p_{xy} = 0$) spin glasses. As temperature increases, the paramagnetic (P) phase appears at the central point, first reaches the transverse spin-glass system and eliminates the spin-glass phase, then reaches the longitudinal spin-glass system and eliminates

the spin-glass phase. Fig.3.3 shows temperature-concentration phase diagrams for isotropically mixed, transverse, longitudinal, and $p_{xy} = 0.5p_z$ spin-glass systems. The upper left and right phase diagrams are seen to be, respectively, reentrant and forward, namely with a ferromagnetic phase that, respectively, recedes from or proceeds towards the spin-glass phase as temperature is lowered, as clearly seen in the insets. The Nishimori symmetry (see below) is obeyed only at four isolated ordinary points in each cross-section in Fig.3.1 and is not obeyed at any point in the phase diagrams in Figs. 3.3, 3.4, so that the forward behavior is not excluded by the rigorous results [3, 4].

A remarkably narrow spin-glass phase, reaching zero-temperature, occurs in the longitudinal spin-glass system. Zero-temperature phase diagrams are shown in Fig.3.4 for the longitudinal (left column) and transverse (right column) spin-glass systems. With the appropriate reversal in variables, the longitudinal and transverse spin-glass phase diagrams are seen to be qualitatively similar, but quantitatively different. The spin-glass phase is more extensive in the transverse case. This can be understood from the more extensive intermixing of the ferromagnetic and antiferromagnetic bonds.

3.4.2 Temperature-Concentration Phase Diagrams with Nishimori Symmetry Curved Lines

The Nishimori symmetry condition [3, 4] for isotropic systems,

$$\frac{1-p}{p} = e^{\pm 2K}, \tag{3.5}$$

generalizes, for uniaxially anisotropic spin-glass systems, to

$$\frac{1-p_{xy}}{p_{xy}} = e^{\pm 2K_{xy}} \quad \text{and} \quad \frac{1-p_z}{p_z} = e^{\pm 2K_z}. \tag{3.6}$$

For Nishimori symmetry to obtain, both equations have to be satisfied, but the signs in the exponents can be chosen independently. The Nishimori condition, in its general form

$$\frac{\mathcal{P}_u(-K_u)}{\mathcal{P}_u(K_u)} = e^{\pm 2K_u} \tag{3.7}$$

for each histogram pair of each distribution, is invariant (closed) under our renormalization-group transformation.

If one of the two conditions in Eq.(3.6) is fixed, phase diagram cross-sections are obtained, in which Nishimori symmetry holds along a line. Thus, throughout the three phase

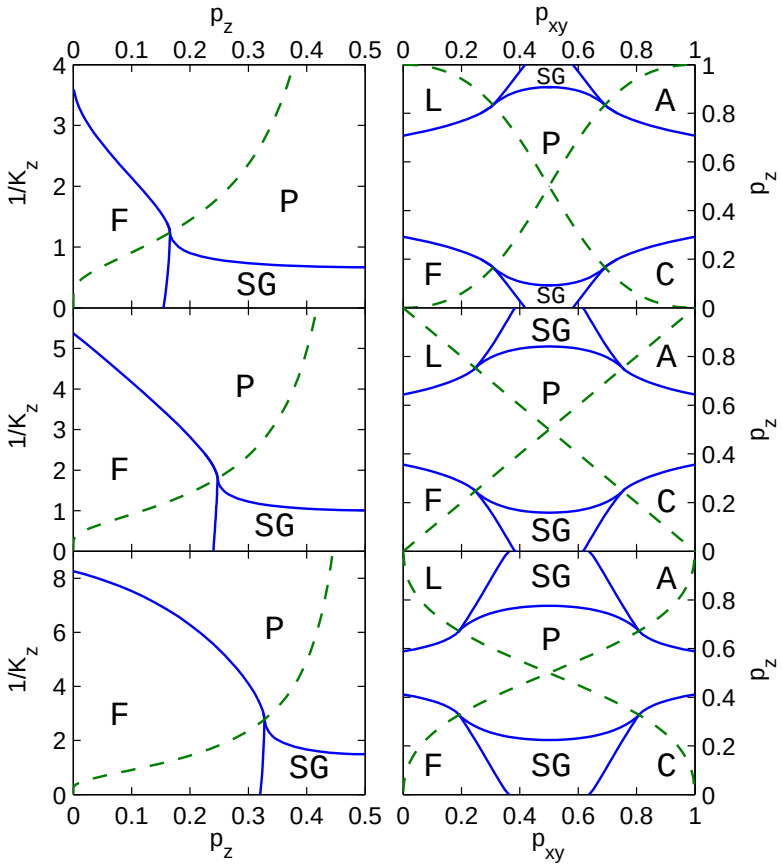

Figure 3.5: Phase diagrams with Nishimori symmetry lines (green dashed) for different anisotropy parameters: The ratio K^z/K^{xy} is 2, 1 and 0.5 from top to bottom. In the left column, p_{xy} satisfies the Nishimori condition. In the right column, K_z satisfies the Nishimori condition. All phase transitions in this figure are second order (blue lines).

diagrams on the left in Fig.3.5, the condition on (K_{xy}, p_{xy}) is fixed. The condition on (K_z, p_z), and therefore Nishimori symmetry, is satisfied along the green dashed lines on the left in Fig.3.5. In these temperature versus concentration phase diagrams, it is seen that the multicritical points between the ferromagnetic, spin-glass, and paramagnetic phases lie on the Nishimori symmetry line. Furthermore, it has been proven [3, 4] that a forward phase diagram cannot occur below such a multicritical point that is on the symmetry line. On the left in Fig.3.5, this is indeed the case, with reentrant phase diagrams, as also seen in isotropic spin glasses [14, 15]. Recall that in Sec.IVA, multicritical points, between the same phases as here, that do not lie on Nishimori symmetry occur with both reentrant and forward phase diagrams. However, the latter non-symmetric multicritical points flow, under

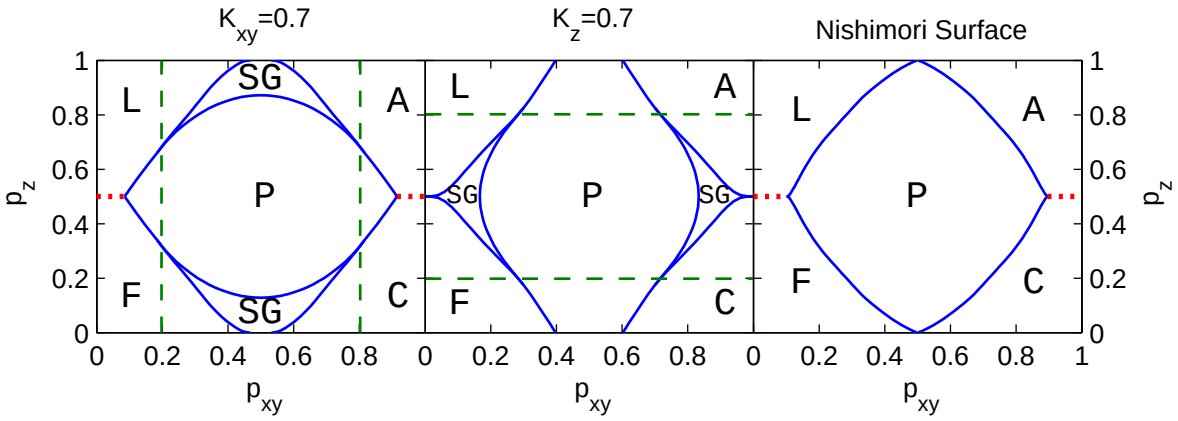

Figure 3.6: The Nishimori condition for K_z is held throughout the leftmost figure and for K_{xy} throughout the center figure. The complimentary Nishimori condition, for K_{xy} and K_z respectively, is held along the green dashed straight lines, which intersect the ordered (F, L, A, or C)-spinglass-paramagnetic multicritical points. In the rightmost figure both conditions are satisfied throughout the figure. In this figure, the phase boundaries around the paramagnetic phase are actually lines of the multicritical points where the paramagnetic, ordered (F, L, A, or C), and spin-glass (not seen in this cross-section) phases meet. In the side figures, first-order boundaries (red dotted) occur between the ferromagnetic and layered phases, and between the antiferromagnetic and columnar phases, terminating at $d = 2$ critical points. All other phase transitions (blue lines) in this figure are second order.

renormalization-group transformations, to the (doubly unstable) fixed distribution of the symmetric multicritical points, therefore being in the same universality class and having the same critical exponents.

In the three phase diagrams on the right of Fig.3.5, the condition on (K_z, p_z) is fixed. In these concentration-concentration phase diagrams, the multicritical points between the ordered (ferromagnetic, antiferromagnetic, layered, or columnar), spin-glass, and paramagnetic phases again lie on the Nishimori symmetry lines.

3.4.3 Concentration-Concentration Phase Diagrams with Nishimori Symmetry Straight Lines

In the phase diagrams in Fig. 3.5, the ratio K_z/K_{xy} is held constant. On the left and center of Fig. 3.6, again the condition in Eq.(3.6) on one interaction is fixed and the other interaction strength is held constant. Thus, the Nishimori symmetry lines becomes straight lines. The multicritical points between the ordered (ferromagnetic, antiferromagnetic, layered, or

columnar), spin-glass, and paramagnetic phases again lie on the Nishimori symmetry lines. In the left phase diagram, due to the enforced Nishimori symmetry condition, $K_z = 0$ along the line $p_z = 0.5$ and the system reduces to $d = 2$. Along this line, first-order transitions between ferromagnetic and layered phases and between antiferromagnetic and columnar phases terminate at $d = 2$ critical points. For $p_z \neq 0.5$, $d = 3$ second-order boundaries between each ordered phase and the paramagnetic phase terminate on the $d = 2$ critical points. In the center phase diagram, due to the enforced Nishimori symmetry condition, $K_{xy} = 0$ along the line $p_{xy} = 0.5$ and the system reduces to $d = 1$. Accordingly, the system is disordered (paramagnetic) along the entire length of this line.

3.4.4 The Phase Diagram Entirely Imbedded in Nishimori Symmetry

In the rightmost Fig. 3.6, both conditions of Eq.(3.6) are satisfied throughout the figure. With two symmetry constraints, this is a unique surface in the global phase diagram of our model. The system reduces to $d = 2$ and $d = 1$, as explained above, for $p_z = 0.5$ and $p_{xy} = 0.5$ respectively. The phase boundaries around the paramagnetic phases are actually lines of the multicritical points where the paramagnetic, ordered (ferromagnetic, layered, antiferromagnetic, or columnar), and spin-glass (not seen in this cross-section) phases meet.

No spin-glass phase occurs within the Nishimori-symmetric subspace. The phase transitions seen in the rightmost Fig. 3.6, namely ordered-spinglass-paramagnetic multicritical and ferromagnetic-layered, antiferromagnetic-layered first-order transitions, are the only phase transitions of the system that occur under Nishimori symmetry.

3.4.5 Fixed Distributions

The fixed distributions underpinning the phase diagrams of this system are given in Fig. 3.7. The fixed distributions for the ferromagnetic-spinglass boundary, paramagnetic-spinglass boundary, and the ferromagnetic-spinglass-paramagnetic multicritical points are spatially isotropic, but attract both spatially isotropic and anisotropic phase transitions. The fixed distribution for the ferromagnetic-spinglass-paramagnetic multicritical points obeys Nishimori symmetry, but attracts multicritical points that obey and do not obey Nishimori symmetry. In the latter cases, as seen above, both reentrant and forward phase diagrams occur.

The fixed distributions for the antiferromagnetic-spinglass, columnar-spinglass, layered-spinglass phase boundaries and for the antiferromagnetic-spinglass-paramagnetic, columnar-spinglass-paramagnetic, layered-spinglass-paramagnetic multicritical points are as shown in Fig.6 (a) and (c) respectively, but with the appropriate $K_{xy} \to -K_{xy}$ and/or $K_z \to -K_z$ reflections.

3.5 Conclusion

The exact solution of the spatially uniaxially anisotropic spin glass on a $d = 3$ hierarchical lattice yields new phase diagrams. In view of the semiquantitative agreement between spatially isotropic spin-glass results on cubic and hierarchical lattices [14], it would certainly be worthwhile to investigate on cubic lattices the new phenomena found in the present study. Furthermore, the exact study of spin glasses on fully anisotropic $d = 3$ hierarchical lattices [41] may yield even more new phase transition phenomena.

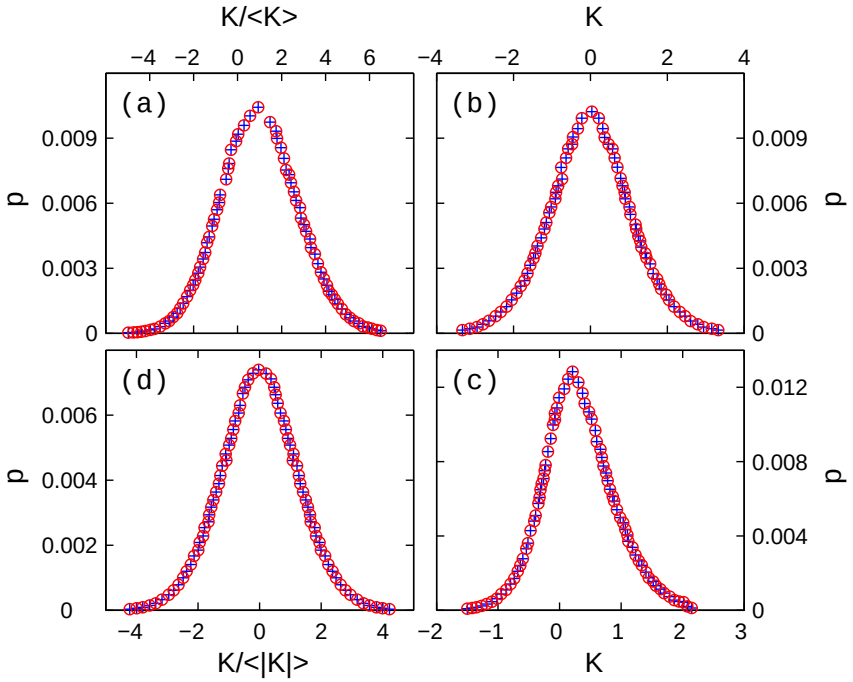

Figure 3.7: Fixed distributions, with circles and crosses showing one renormalization-group transformation and thereby by their exact superposition attesting to the fixed nature of the distributions. The distributions have been binned for exhibition purposes. (a) For the ferromagnetic-spinglass phase boundary, a runaway to infinite coupling; (b) for the paramagnetic-spinglass phase boundary. Both of these fixed distributions are spatially isotropic, attracting isotropic and anisotropic boundaries, and do not obey Nishimori symmetry. (c) For the ferromagnetic-spinglass-paramagnetic multicritical point. This fixed distribution is spatially isotropic and obeys Nishimori symmetry. This fixed distribution attracts the isotropic multicritical point, which obeys Nishimori symmetry, and anisotropic multicritical points, which obey and do not obey Nishimori symmetry. The fixed distributions for the antiferromagnetic-spinglass, columnar-spinglass, layered-spinglass phase boundaries and for the antiferromagnetic-spinglass-paramagnetic, columnar-spinglass-paramagnetic, layered-spinglass-paramagnetic multicritical points are as shown here in (a) and (c) respectively, but with the appropriate $K_{xy} \to -K_{xy}$ and/or $K_z \to -K_z$ reflections. (d) Fixed distribution for the spin-glass phase. This phase sink is an isotropic runaway, attracting both spatially isotropic and anisotropic spin-glass phase points, and does not obey Nishimori symmetry.

BIBLIOGRAPHY

[1] M. E. Fisher, Rev. Mod. Phys. **70**, 653 (1998).

[2] H. Nishimori, Statistical Physics of Spin Glasses and Information Processing (Oxford Science Publications, Oxford University Press, 2001).

[3] H. Nishimori, J. Phys. C **13**, 4071 (1980).

[4] H. Nishimori, Prog. Theor. Phys. **66**, 1169 (1981).

[5] H. Nishimori, J. Phys. Soc. Japan **55**, 3305 (1986).

[6] Y. Ozeki and H. Nishimori, J. Phys. A **26**, 3399 (1993).

[7] H. Nishimori, Physica A **205**, 1 (1994).

[8] H. Nishimori and K. Nemoto, J. Phys. Soc. Japan **71**, 1198 (2002).

[9] J.-M. Maillard, K. Nemoto, and H. Nishimori, J. Phys. A: Math. Gen. **36**, 9799 (2003).

[10] K. Takeda and H. Nishimori, Nucl. Phys. B **686**, 377 (2004).

[11] K. Takeda, T. Sasamoto, and H. Nishimori, J. Phys. A: Math. Gen. **38**, 3751 (2005).

[12] M. Hinczewski and A.N. Berker, Phys. Rev. B **72**, 144402 (2005).

[13] H. Nishimori, J. Stat. Phys. **126**, 977 (2007).

[14] G. Migliorini and A.N. Berker, Phys. Rev. B **57**, 426 (1998).

[15] F.D. Nobre, Phys. Rev. E **64**, 046108 (2001).

[16] M. Ohzeki, J. Phys. Soc. Japan **76**, 114003 (2007).

[17] M. Hinczewski and A.N. Berker, Eur. Phys. J. B **51**, 461 (2006).

[18] M. Hinczewski and A.N. Berker, Phys. Rev. B, in press (2008).

[19] A.N. Berker and S. Ostlund, J. Phys. C **12**, 4961 (1979).

[20] R.B. Griffiths and M. Kaufman, Phys. Rev. B **26**, 5022R (1982).

[21] M. Kaufman and R.B. Griffiths, Phys. Rev. B **30**, 244 (1984).

[22] S.R. McKay, A.N. Berker, and S. Kirkpatrick, Phys. Rev. Lett. **48**, 767 (1982).

[23] C. Monthus and T. Garel, Phys. Rev. B **77**, 134416 (2008).

[24] A. Falicov, A.N. Berker, and S.R. McKay, Phys. Rev. B **51**, 8266 (1995).

[25] E. Domany, S. Alexander, D. Bensimon, and L.P. Kadanoff, Phys. Rev. B **28**, 3110 (1983).

[26] J.-M. Langlois, A.-M.S. Tremblay, and B.W. Southern, Phys. Rev. B **28**, 218 (1983).

[27] R.B. Stinchcombe and A.C. Maggs, J. Phys. A **19**, 1949 (1986).

[28] R.F. Angulo and E. Medina, J. Stat. Phys. **75**, 135 (1994).

[29] T.A.S. Haddad, S.T.R. Pinho, and S.R. Salinas, Phys. Rev. E **61**, 3330 (2000).

[30] J.-X. Le and Z.R. Yang, Phys. Rev. E **69**, 066107 (2004).

[31] R.A. da Silveira and J.-P. Bouchaud, Phys. Rev. Lett. **93**, 015901 (2004).

[32] L.-H. Tang and H. Chaté, arXiv:cond-mat/0007350v1 [cond-mat.stat-mech].

[33] M. Hinczewski and A.N. Berker, Phys. Rev. E **73**, 066126 (2006).

[34] M. Hinczewski, Phys. Rev E **75**, 061104 (2007).

[35] Z.Z. Zhang, L.L. Rong, and S.G. Zhou, Physica A **377**, 329 (2007).

[36] Z.Z. Zhang, S.G. Zhou, and T. Zou, Eur. Phys. J. B **56**, 259 (2007).

[37] Z.Z. Zhang, Z.G. Zhou, and L.C. Chen, Eur. Phys. J. B **58**, 337 (2007).

[38] H.D. Rozenfeld, S. Havlin, and D. ben-Avraham, New J. Phys. **9**, 175 (2007).

[39] H.D. Rozenfeld and D. ben-Avraham, Phys. Rev. E **75**, 061102 (2007).

[40] E. Khajeh, S.N. Dorogovtsev, and J.F.F. Mendes, Phys. Rev. E **75**, 041112 (2007).

[41] A. Erbaş, A. Tuncer, B. Yücesoy, and A.N. Berker, Phys. Rev. E **72**, 026129 (2005).

VITA

CAN GÜVEN was born in Konya, Turkey on January 2, 1984. He received his B.Sc. degree in Physics Engineering from Istanbul Technical University, Istanbul, in 2006. He joined Prof. A. Nihat Berker' s research group in his last year of undergraduate studies. From August 2006 to August 2008, he worked as a teaching assistant in Koç University, Turkey and continued his research on anisotropic spin-glasses under the supervision of Prof. A. Nihat Berker and Dr. Michael Hinczewski. He has a joint paper with his supervisors and Prof. Hidetoshi Nishimori, published in the Physical Review E. He is currently working on the tensor renormalization-group approach to disordered systems.